School of Marine Science and Ocean Engineering

Institute for the Study of Earth, Oceans, and Space (EOS)

# Calibration of a general optical equation for remote sensing of suspended sediments in a moderately turbid estuary

Richard P. Stumpf
*U.S.G.S.*

Jonathan Pennock
*University of New Hampshire - Main Campus*

### Recommended Citation

# Calibration of a General Optical Equation for Remote Sensing of Suspended Sediments in a Moderately Turbid Estuary

RICHARD P. STUMPF

*National Oceanic and Atmospheric Administration, National Environmental Satellite, Data, and Information Service, Washington, D.C.*

JONATHAN R. PENNOCK[1]

*College of Marine Studies, University of Delaware, Lewes, Delaware*

A general algorithm for determining suspended sediment concentrations in the surface waters of estuaries has been developed for use with satellite data. The algorithm uses a three-parameter general optical equation to relate suspended sediment concentrations to water reflectances that have been corrected for sun angle effects, atmospheric path radiance, and tidal excursion. Using data collected by the advanced very high resolution radiometer on five different dates, reflectances were determined using two different methods, one providing maximum correction for haze and the other providing minimum sensitivity to pigments. For both methods, in situ and remotely sensed samples from Delaware Bay acquired within 3.5 hours of each other agreed to within 60% at the 95% confidence level. Pixel and subpixel scale spatial variations and variability associated with in situ measurements produced about 50% of the differences. Chlorophyll concentrations of >50 $\mu$g/L produced a discrepancy in the reflectance method that provided the best haze correction. The parameter values may be adjusted to allow for variations in sediment size and pigment variations, allowing application of the calibration to estuaries having optically different suspended sediments.

## INTRODUCTION

The distribution and transport of suspended sediments is a major concern in the study of estuaries and many coastal regions. The amount of suspended matter changes rapidly with fluctuations in tides, winds, and river discharge and shows considerable spatial variability. This variability makes shipboard data collection for many monitoring and modeling purposes extremely expensive and logistically complex.

Data obtained from satellites can provide some of the synoptic data needed to study suspended sediments in estuaries. Several researchers have shown that total suspended matter or seston can be correlated with radiance data collected from satellite: for example, Landsat multispectral scanner (MSS) [*Klemas et al.*, 1974; *Munday and Alfoldi*, 1979; *Khorram*, 1985; *Ritchie et al.*, 1987; *Stumpf*, 1988a], the coastal zone color scanner (CZCS) [*Tassan and Sturm*, 1986], and the advanced very high resolution radiometer (AVHRR) [*Curtin and Legeckis*, 1986; *Stumpf*, 1987].

For the study of temporal changes in estuarine sediment loads and for the comparison of different estuaries, several problems must be resolved. Comparisons of data collected on different dates require correction for differences in sun angle and atmospheric path radiance, as has been shown by several researchers [*Munday and Alfoldi*, 1979; *MacFarlane and Robinson*, 1984; *Tassan and Sturm*, 1986; *Stumpf*, 1988a,b]. Second, an atmospheric correction that can remove haze patterns within a scene should be available [*Stumpf*, 1988b].

In addition, the calibration equation should be derived physically rather than statistically, to permit comparisons with in situ optical measurements and to account for compositional changes. Finally, the equation should be of a sufficiently general form to reduce the amount of recalibration data needed for application to different scenes, sensors, and estuaries.

Following the work of *Munday and Alfoldi* [1979], *Stumpf* [1987, 1988b] has developed a calibration equation that satisfies the latter points: a physical basis and a potentially general form. We will here examine the procedure for calibrating that equation and its potential for accurately representing the suspended sediment concentrations over a period of several months using AVHRR data collected for Delaware Bay.

## SATELLITE CHARACTERISTICS

The AVHRR is on board the NOAA TIROS-N (Television and Infrared Observation Satellite) platforms, which are polar-orbiting and sun-synchronous satellites that have one daytime and one nighttime pass each day. Of the series (designated NOAA 6 through NOAA 11), NOAA 9 and NOAA 10 were operational during the study period. Daytime overpasses occurred about 0745–0830 local standard time for NOAA 10, and about 1400–1500 local standard time for NOAA 9. Although the morning sun produces less illumination of NOAA 10 scenes, there is generally sufficient illumination during the period from midspring to midsummer to produce acceptable scene quality at mid-latitudes.

The AVHRR has two channels that detect reflected light: channel 1, which detects red light (0.58–0.68 $\mu$m), and channel 2, which detects near-infrared light (0.72–1.0 $\mu$m). The detected spectral bands are comparable to those on the sensors of other satellites, including Landsat and SPOT (The French systeme probatoire d'observation de la Terre),

permitting application of the techniques described here to data from these other sources [e.g., *Stumpf*, 1988b]. The AVHRR also has a radiometric resolution and dynamic range favorable for studying moderately turbid to highly turbid waters [*Gagliardini et al.*, 1984]. Having been designed for cloud and snow analyses (as well as for sea surface temperature [*Strong and McClain*, 1984]), the sensor also responds rapidly and stably to large shifts in the incoming signal, such as the change from land to water. *Kidwell* [1986] and *Planet* [1979] describe the AVHRR specifications and data sets in greater detail.

## DETERMINATION OF SUSPENDED SOLIDS

A physical model describing the reflectance from the water column provides the most effective way to analyze remotely sensed data for suspended sediments. Several methods of solving the radiative transfer equation have been developed to relate irradiant reflectance to the optical properties of a deep, vertically homogeneous water column [*Gordon et al.*, 1975; *Jain and Miller*, 1977; *Philpot*, 1987]. The resultant equations are similar in form. Using the solution of *Gordon et al.* [1975] this form may be expressed as

$$R_{-}(\lambda) = Y \frac{b_b(\lambda)}{a(\lambda) + b_b(\lambda)} \qquad (1)$$

where $R_{-}$ is the irradiant reflectance just below the water's surface; $\lambda$ is the spectral band; $b_b$ is the backscatter coefficient; $a$ is the absorption coefficient; and $Y$ is a constant, which *Gordon et al.* suggest is equal to 0.33. $R_{-}$ is about 1.85 times greater than the reflectance just above the surface $(R)$ owing to refraction and reflection of the upwelling radiance at the water's surface.

For remote sensing in turbid water where backscatter from sediment is much greater than backscatter from the water, (1) can be rewritten as

$$R(\lambda) = \frac{Y_1 b_{bs}^*(\lambda)}{s^*(\lambda) + a_x(\lambda)/n_s} \qquad (2)$$

where

$$s^*(\lambda) \equiv a_s^*(\lambda) + b_{bs}^*(\lambda)$$

$$a_x(\lambda) \equiv a_w(\lambda) + a_d^*(\lambda)n_d + a_p^*(\lambda)n_p$$

and where $Y_1$ is a constant equal to 0.18 that incorporates the constant $Y$ (=0.33) in (1) and the water surface and radiance distribution effects; $n$ denotes concentrations; $a$ denotes absorption coefficients, $b_b$ denotes backscatter coefficients; the subscripts $s$, $w$, $d$, and $p$ denote sediment, water, dissolved pigments, and particulate pigments such as chlorophyll, respectively, and the superscript asterisks denote specific absorption or backscatter coefficients [*Stumpf*, 1987].

With in situ data for the suspended sediment concentration $n_s$ and remotely sensed data for the reflectances, we can find $b_{bs}^*$, $s^*$, and $a_x$ using a best fit solution to (2). Unlike statistically derived equations relating reflectance and sediment concentration [*Klemas et al.*, 1974; *Khorram*, 1985], (2) allows for the effects of variations in the composition of the suspended matter on the coefficients.

Variations in the optical grain size of the sediment can alter both $s^*$ and $b_{bs}^*$ for all wavelengths in a predictable manner [*Stumpf*, 1988b; *vande Hulst*, 1957]. For example, an increase in size will produce a decrease in these values owing to the decrease in the ratio of surface area to mass. Increased pigment absorption, predominately by chlorophyll and phycocyanin, will reduce the AVHRR channel 1 reflectance by increasing $a_x$. Inorganic pigments, especially iron compounds, may also reduce reflectance through increasing $s^*$, although primarily for the blue and green wavelengths where these compounds have the greatest absorption. Only extremely high concentrations of iron oxides and other red pigments should influence the reflectances for the red and near-IR bands, making these the preferred spectral bands for examining sediment in turbid water.

## ATMOSPHERIC CORRECTION

Reflectance is determined from remotely sensed radiances through corrections for variations in the incident irradiance and the atmospheric conditions; the corrections have been described by several authors [*Gordon et al.*, 1983; *MacFarlane and Robinson*, 1984; *Stumpf*, 1988b]. The approach outlined here follows that presented by *Stumpf* [1988b] and is similar to the technique applied to CZCS data by *Gordon et al.* [1983].

Reflectance $(R)$ at the water's surface is determined as

$$R(\lambda) \equiv \frac{E_u(\lambda)}{E_d(\lambda)}$$

$$= \frac{Q L_w(\lambda)}{E_o(\lambda) \cos \theta_o \ \exp\{-[\tau_r(\lambda)/2 + \tau_{oz}(\lambda)]/\cos \theta_o\}} \qquad (3)$$

where $\lambda$ is the spectral band or wavelength; $E_u$ and $E_d$ are the upwelling and downwelling irradiances just above the water's surface (for $R_{-}$ the irradiances immediately below the surface are used), $E_o$ is the solar irradiance at the top of the atmosphere, $L_w$ is the radiance from the water, $Q$ is a constant of proportionality here assigned equal to $\pi$, and $\theta_o$ is the solar zenith angle. Transmission losses of the incident solar irradiance are accounted for by the exponential term, wherein $\tau_r$ is the optical depth for Rayleigh scattering and $\tau_{oz}$ is that for molecular absorption by ozone and water vapor.

The radiance from the water column, $L_w$, can be found from the radiance received at the sensor $(L_*)$ using

$$L_w(\lambda) = [L_*(\lambda) - L_A(\lambda)] / T_1(\lambda) - L_g(\lambda) \qquad (4)$$

where $L_A$ is the atmospheric path radiance, $L_g$ is the radiance reflected from the water surface (i.e., sun glint), and $T_1$ is the atmospheric diffuse transmission coefficient from the Earth to the satellite. Outside of regions containing sun glint, $L_g$ can be ignored. In sun glint regions, *Stumpf* [1987] describes a technique to obtain reflectances in the presence of the glint. $L_A$ can be found from

$$L_A(\lambda) = L_r(\lambda) + L_a(\lambda) \qquad (5)$$

where $L_r$ is the Rayleigh radiance and $L_a$ is the aerosol (haze) radiance. $L_a$ is estimated using the radiance over clear water

near the Bay [*Stumpf*, 1987]. $L_r$ is determined using the formulation

$$L_r(\lambda) = E_o(\lambda) \ \exp\{-\tau_{oz}(\lambda) \ / \cos \theta_1\} \ \tau_r(\lambda) \ P_r(\varphi) \ / \cos \theta_1 \tag{6}$$

where $P_r(\varphi)$ is the Rayleigh scattering phase function for the scattering angle $\varphi$ (from sun to atmosphere to sensor) [*Gordon et al.*, 1983]. Secondary Rayleigh scattering effects (i.e., from surface to atmosphere to sensor) are not calculated as they are small in relation to the turbid water signal, particularly for the longer (red and near-IR) wavelengths favored here.

The atmospheric transmission $T_1$ is found from

$$T_1(\lambda) = \exp\{-[\tau_a(\lambda) + \tau_r(\lambda)/2 + \tau_{oz}(\lambda)] / \cos \theta_1\} \tag{7}$$

where $\tau_a$ is found from a linear relationship to $L_a$ [*Griggs*, 1983; *Durkee*, 1984; *Stumpf*, 1988b].

Near-IR radiation is strongly absorbed by water, thereby producing a weak signal when compared to aerosol variations. In addition, the red spectral band is somewhat sensitive to variations in pigment absorption. Thus combining data for the two spectral bands will reduce the effects of pigments while increasing the strength and sensitivity of the signal to suspended sediment. This combined reflectance is found from

$$R_T = \frac{Q \ [L_w(1) + L_w(2)]}{[E_d(1) + E_d(2)]} \tag{8}$$

with $Q$ equal to $\pi$; $L_w$ determined from (4); $E_d$ expressed in (3); and 1 and 2 denoting channel 1 (red band) and channel 2 (near-IR band) on the AVHRR. $R_T$ can be used as a measure of the water's turbidity or can be used with (2) to find the suspended sediment concentrations $n_s$. It can be considered an albedo measurement for the red and near-infrared region.

When variable haze patterns lie over the area of interest, the assumption of constant $L_a$ can result in spatial distortions in $R_T$ or $R(\lambda)$. Aerosol contamination may vary considerably within a scene, therefore a pixel-by-pixel correction would more effectively reduce $L_a$. One solution takes advantage of $R(1)$ being generally much greater than $R(2)$ for water [*Stumpf*, 1987]. We could obtain an aerosol correction at each pixel through the reflectance difference

$$R_D = R(1) - A \ R(2) \tag{9}$$

where $R$ is found from (3) and $A$ is a constant determined by the aerosol spectral relationship between $R(1)$ and $R(2)$. For larger aerosol particles such as those found in clouds, $A$ approximately equals 1.0 [*Durkee*, 1984]. Different aerosol types in a scene may have different values of $A$. A value for $A$ of 1.0 appears to remove the effects of most common aerosols, therefore it is used routinely here. (In addition, $A$ = 1.0 removes sunglint contamination as described by *Stumpf* [1987].) $R_D$ will then remove much of the aerosol contamination, leaving the signal derived from the water column. The application of $R_D$ should produce consistent results in studies involving large areas or multiple scenes.

## METHODS

### Satellite Data Processing

The AVHRR data sets were acquired in digital form on NOAA level 1B data tapes (see *Kidwell* [1986] for details). The tapes were processed through the NOAA NESDIS (Washington, D.C.) software to determine reflectances (and sea surface temperatures) and to map the data to a Mercator projection with a pixel size of 1.16 km at 39°N. The navigation data supplied on the tapes produced positioning errors of 2-10 pixels. To correct for this effect, the images were linearly shifted to correct the coastline pixels to within 1 pixel of their true position. The images were finished and values extracted using a programs developed within a commercial software package (EASI/PACE developed by PCI, Inc. of Toronto, Canada).

### In Situ Observations

The suspended sediment and chlorophyll measurements were collected as part of the SCENIC series of cruises in Delaware Bay during the Spring of 1987 (Figure 1). Vertical profiles of salinity, temperature, and transmissivity were collected using a Neil Brown Mark IIIb conductivity-temperature-depth profiler. Surface water samples were obtained by Niskin bottle within 1 m of the surface. Suspended sediment concentrations, or more generally, total seston, were determined by filtration onto tared 1.0-$\mu$m Nuclepore filters that were dried under vacuum and reweighed [*Sharp et al.*, 1982]. Replicates of $n_s$ indicate an accuracy within 10% for these in situ samples. Chlorophyll-$a$ concentrations were determined fluorometrically following the procedure of *Strickland and Parsons* [1972]. The diffuse attenuation coefficient k was determined as was described by *Pennock* [1985] using a quantum radiometer. The specific diffuse attenuation coefficient for sediment was determined by linear regression of k against $n_s$. *Pennock* [1985] gives additional information on the data collection procedures.

### Calibration Procedure

The in situ observations were collected during cruises SC-7 (March 5-6, 1987), SC-8 (March 22, 1987), SC-10 (April 29-30, 1987), and SC-11 (May 28, 1987). Table 1 describes the AVHRR overpasses. Except for some in situ samples collected on April 29 (AVHRR digital data sets were missing on this date) all comparisons of in situ and remotely sensed data were made using observations taken on the same day and generally within 3 hours of an overpass. Additionally, all the comparisons included only satellite data from the lower estuary, where the width exceeds 4 pixels, thereby avoiding shoreline effects.

It is difficult to obtain shipboard data at exactly the time of a satellite overpass. Because of strong tidal currents in the Delaware estuary, differences in time between the shipboard samples and the synoptic satellite image will result in a varying offset in the position of the sampled water relative to its position in the image. To correct for tidal transport between the image time and the sample time, sample station locations were adjusted in the imagery. The predicted stages of the tidal currents were determined from the tidal current tables [*U.S. Department of Commerce*, 1987] for the period between
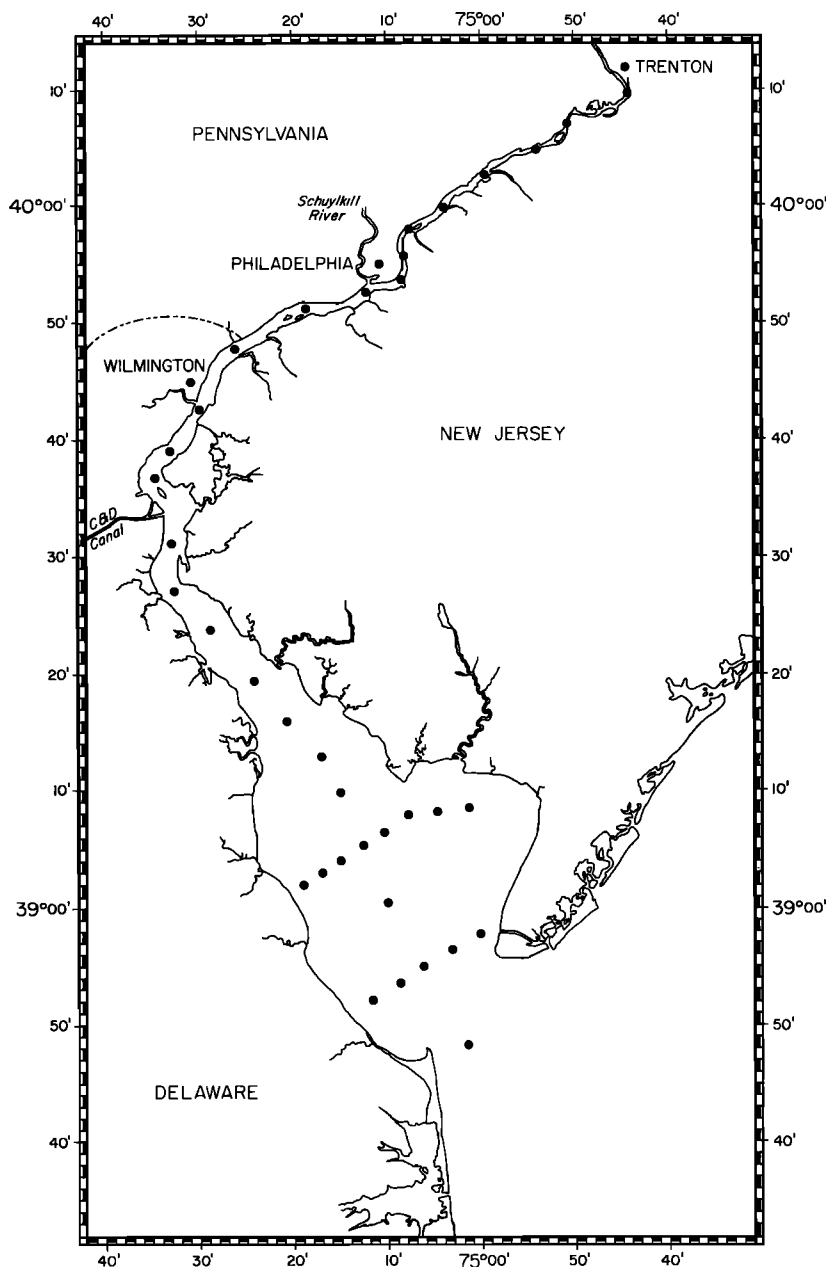
Fig. 1. Locations of sampling stations in Delaware Bay.

TABLE 1. AVHRR Overpasses Used in This Study

| Satellite | Date | Time | Orbit |
|---|---|---|---|
| NOAA 9 | March 5, 1987 | 1445 | 11474 |
| NOAA 9 | March 6, 1987 | 1435 | 11488 |
| NOAA 9 | March 22, 1987 | 1505 | 11742 |
| NOAA 10 | April 30, 1987 | 0750 | 3197 |
| NOAA 9 | May 28, 1987 | 1445 | 12659 |

Times are in eastern standard time.

the sample time and image time. The mean current (approximately 2 km/hour) was multiplied by the time between the two samples to give the translation of the sampled water. For the hour before and after slack water, the current was assumed negligible. On the basis of the tidal current tables, the direction of motion was assumed parallel to the bay axis (NW-SE) for stations near the axis, where the majority of the water samples were collected. For stations nearer New Jersey, the direction of motion is more northerly or southerly; for stations near the Delaware shore it is more westerly or easterly.

The amount and direction of adjustment from the station location gave the pixel used to correspond to the water sampled from ship. The median reflectance value of the 3x3 block of pixels centered on this pixel was compared with the in situ data.

Determination of $b_{bs}*$, $s*$, and $a_x$ involved fitting (2) to plots of the observations of reflectance (either $R_T$ or $R_D$) against $n_s$. The procedure used the Marquardt-Levenberg method of least squares approximation as applied in the RS/1 statistical analysis package (developed by Bolt, Beranek, and Newman [1981]). These cases used $Y_1$ = 0.18 (0.33/1.85), where 1.85 incorporates water surface refraction and reflection discussed earlier.

## DISCUSSION

The conditions investigated here include suspended sediment (seston) concentrations ranging from 3.5 to 62 mg/L. Chlorophyll concentrations varied from 3 $\mu$g/L to 81 $\mu$g/L, the high values due to the annual spring phytoplankton bloom. These ranges are typical for other U.S. estuaries, such as Chesapeake Bay [Schubel, 1972] and San Francisco Bay [Arthur and Ball, 1979; Cole et al., 1986].

### Predictive Potential

Equation (2), when fitted to all of the data for $R_T$ and $n_s$ (n=45), accounts for 90% of the variance from the mean in $R_T$. Restricting the data to measurements taken less than 3.5 hours from an overpass (all but three samples were collected within 3 hours) further improves the fit to (2), accounting for over 98% of the variance (Figure 2). For this data set, different sampling dates and changes in chlorophyll concentration have minimal effects on the relation of $R_T$ to $n_s$.
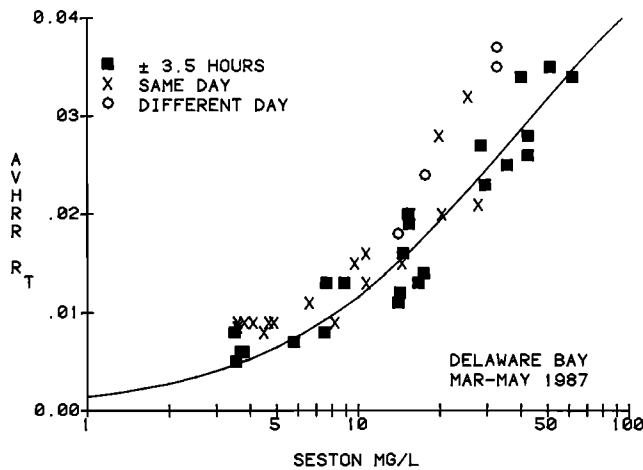


Fig. 2. Seston (suspended sediment) concentrations versus $R_T$ reflectance in Delaware Bay. Seston values are from cruises in March, April, and May, 1988 aboard the R/V Cape Henlopen. Reflectance values are from AVHRR overpasses. The solid line is the best fit solution to equation (2) for the samples collected within 3.5 hours.

Equation (2) also explains over 98% of the variance between $R_D$ and $n_s$ for chlorophyll concentrations of less than 50 $\mu$g/L (Figure 3). When samples containing higher chlorophyll concentrations are included, the relationship weakens. Chlorophyll-like pigments and extremely high concentrations of dissolved pigments increase the absorption coefficient $a_x$ of red light, thereby decreasing $R(1)$ without affecting $R(2)$ [Stumpf and Tyler, 1988; Stumpf, 1988b]. Hence the value of $R_D$ varies with the presence of these pigments. Because $R_T$
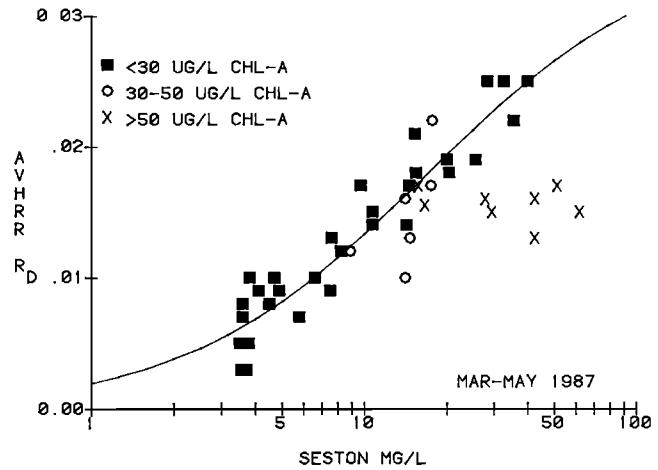


Fig. 3. Seston (suspended sediment) concentrations versus $R_D$ reflectance for the same samples as in Figure 2. The data pairs are plotted according to chlorophyll concentration. The solid line is the best fit solution of (2) for the samples having chlorophyll concentrations of <50 $\mu$g/L.

involves an addition of data from the two bands, the channel 2 radiances reduce the impact of the fluctuations in the channel 1 radiances. $R_D$ and $R_T$ can be equal under certain conditions, namely when the color index $C_{21}$ has a value of 0.3. ($C_{21}$ is defined as the reflectance ratio $\Delta R(2)/\Delta R(1)$, where $\Delta R$ is the reflectance deviation from the clear water reflectance [Stumpf and Tyler, 1988] and the clear water reflectance is negligible for red and near-infrared light.) However, when $C_{21}$ increases, as with increasing pigment concentrations, $R_D$ becomes less than $R_T$. This change in $R_D$ appears as a deviation below the curve in Figure 3. For a uniform color index, $R_D$ behaves like $R(1)$. Namely, by including $C_{21}$ in (9), we have

$$R_D = R(1) \ (1 - A \ C_{21}) \qquad (10)$$

For $C_{21}$ about 0.4, which is common in the middle Atlantic estuaries [Stumpf and Tyler, 1988], $R_D$ corresponds to approximately 0.6 $R(1)$.

The coefficients determined from the fit of (2) to the data are shown in Table 2. The fit of the inverted form of (2), i.e., $n_s$ in terms of $R_T$, has a somewhat lower F value (the ratio of explained to residual sums of squares). This results from the increased sensitivity of the inverted form to the tails in the logistic curve. Slight changes in reflectance produce proportionately greater changes, or residuals, in $n_s$ in these regions than in the center of the curve.

The coefficients for $R_T$ are similar to estimates determined from other methods (Table 3). In addition, the estimates of $k_s*$ from the reflectance data corresponds to $k_s*$ determined solely from the in situ data. The similar ranges of the coefficients from (2) with those determined in other studies supports the argument that the parameters in (2) have a physical meaning. For $R_D$, although the coefficients will have some physical meaning, they may tend to have slightly distorted values as compared with those for $R_T$ because $R_D$ is similar to but not the same as $R(1)$. As noted earlier, $R_D$ is approximately equal to 0.6 $R(1)$, forcing $s*$ to increase relative to $b_{bs}*$ to produce this effect.

TABLE 2. Coefficients Determined for Equation (2) from
the Delaware Estuary Data, March-May, 1987

| | $R_T$ | $R_D$ for <30 $\mu g/L$ Chl-$a$ | $R_D$ for <50 $\mu g/L$ Chl-$a$ | $R_T$ for inverted form of (2) |
|---|---|---|---|---|
| $b_{bs}$*, m²/mg | 0.018 | 0.024 | 0.022 | 0.020 |
| $s$*, m²/mg | 0.056 | 0.120 | 0.110 | 0.049 |
| $a_x$, m⁻¹ | 2.2 | 1.8 | 1.9 | 3.0 |
| No. of Samples | 23 | 31 | 37 | 23 |
| $r^2$ | 0.98 | 0.98 | 0.98 | 0.98 |
| F value | 326 | 521 | 486 | 166 |

TABLE 3. Specific Attenuation and Backscatter Coefficients

| | Delaware Bay From (2) | Delaware Bay Ship | Other Work |
|---|---|---|---|
| $b_{bs}$*, m²/mg | 0.018 | 0.008-0.027 [a] | 0.01-0.05 [b,c] |
| $s$*, m²/mg | 0.056 | | 0.055 [c] |
| $a_x$ (m⁻¹) | 2.2 | | 1.5 [d] |
| $k_s$* (m²/mg) | 0.079 [f] | 0.074 [e] | |

[a] *Lyzenga et al.* [1988].
[b] *Whitlock et al.* [1981].
[c] *Bukata et al.* [1981].
[d] *Curcio and Petty* [1951].
[e] This study.
[f] Here, $k_s$* = 1.3$as$* + $b_{bs}$* (based on *Philpot* [1987]).

The logistic form of (2) explains the success of the logarithmic relationship ($R$ versus log($n_s$)) presented by several researchers [e.g., *Klemas et al.,* 1974; *Munday and Alfoldi,* 1979]. However, (2) provides a superior representation of the relationship, as a logarithmic relationship would plot as a straight line in Figure 2, missing the tail at low $n_s$ seen here and the apparent tail and asymptotic response in reflectance at high $n_s$ seen in other data sets [e.g., *Stumpf,* 1988b].

A preference for either $R_T$ or $R_D$ will depend on environmental conditions. Under variably hazy or cloudy conditions, $R_D$ will reduce spatial fluctuations in the aerosol component, giving usable results over a broader area. As is shown in Figure 4, depicting the middle Atlantic coast on May 10, 1988, $R_T$ contains aerosol contamination, especially in the southern portion of the image. However, these distortions have been removed in the image showing $R_D$. The reduced distortion by haze makes $R_D$ more suitable for use with a large number of scenes or large areas. However, $R_T$ can provide more meaningful results for individual scenes containing strong variations in water color and minimal aerosol contamination.

*Error Analysis*

Figure 5 compares the suspended sediment concentrations estimated from the logistic equation (2) with the observed concentrations. At the 95% confidence level, the samples collected within 3.5 hours lie within 60% of an exact match. The good fit for these samples indicates that errors for samples collected more than 3.5 hours apart result primarily from the differences in sampling times, not from problems in the model or the remotely sensed data. Hence these estimated concentrations may accurately represent $n_s$ at the time of overpass.

The importance of correcting for movement of the sampled water will depend on the amount of movement and the areal variation in the reflectance field. Although, in general, the corrected and uncorrected data sets overlap (Figure 6), some uncorrected points fall well away from the bulk of the data. In particular, at higher $n_s$, the $R_T$ values for the uncorrected positions tended to be lower than those for the corrected positions. (Not all samples have both corrected and uncorrected values; the position shift moved some locations either into or away from the narrow upper estuary or from areas obscured by clouds.) This bias could be either negative, as occurred here, or positive, depending on the reflectance field and tidal stage during sampling. In several cases, the movement of turbidity fronts brought clearer water to the position of the ship station before the satellite overpass occurred.

After temporal and translational variability are considered, some discrepancies remain in the 3.5-hour data set. These discrepancies have sources in both the remotely sensed and the in situ data (Table 4). In the remotely sensed data, errors may arise in the calculation of $R_T$ and $R_D$ or in the identification of the correct pixel. Determination of $L_a$, the aerosol path radiance, may cause the greatest error in calculating the reflectance. Under good atmospheric conditions, $R_T$ can vary by about 0.003 in regions where no signal from the water is expected (e.g., offshore). This variation will produce a real error of as much as 20% in the estimated $n_s$ between 10 and 70 mg/L. For the tail, where $n_s$ is less than 10 mg/L, atmospheric variability would produce a somewhat larger percentage error.

In most cases, values in the 3x3 box of pixels were within 0.002 of the median value. This deviation could correspond to a variation of 10% in $n_s$ between 10 and 70 mg/L. This component incorporates two main classes of error: (1) digitization error and noise in the sensor, and (2) positioning errors. The median value will eliminate most random noise, leaving the digitization error. Positioning error involves finding the correct reflectance value based on the accuracy of determining not only the true location of the pixels but also the true location of the sampled water. These two sources of positioning error cannot be easily separated because both have the same effect and both covary with the areal variability of $n_s$. Subpixel scale variability in the suspended sediment field may also be an important source of variance in the data. The in situ measurement takes a sample representative of a Niskin bottle having a cross-sectional area of about 100 cm², whereas the satellite pixel represents an area of 1.35 km². We were able to make a conservative estimate of the variability in the sediment field using transmissometer tracklines. A Hydroproducts 612A white light transmissometer (10-cm path length) was installed in a bath connected to a through-hull pump
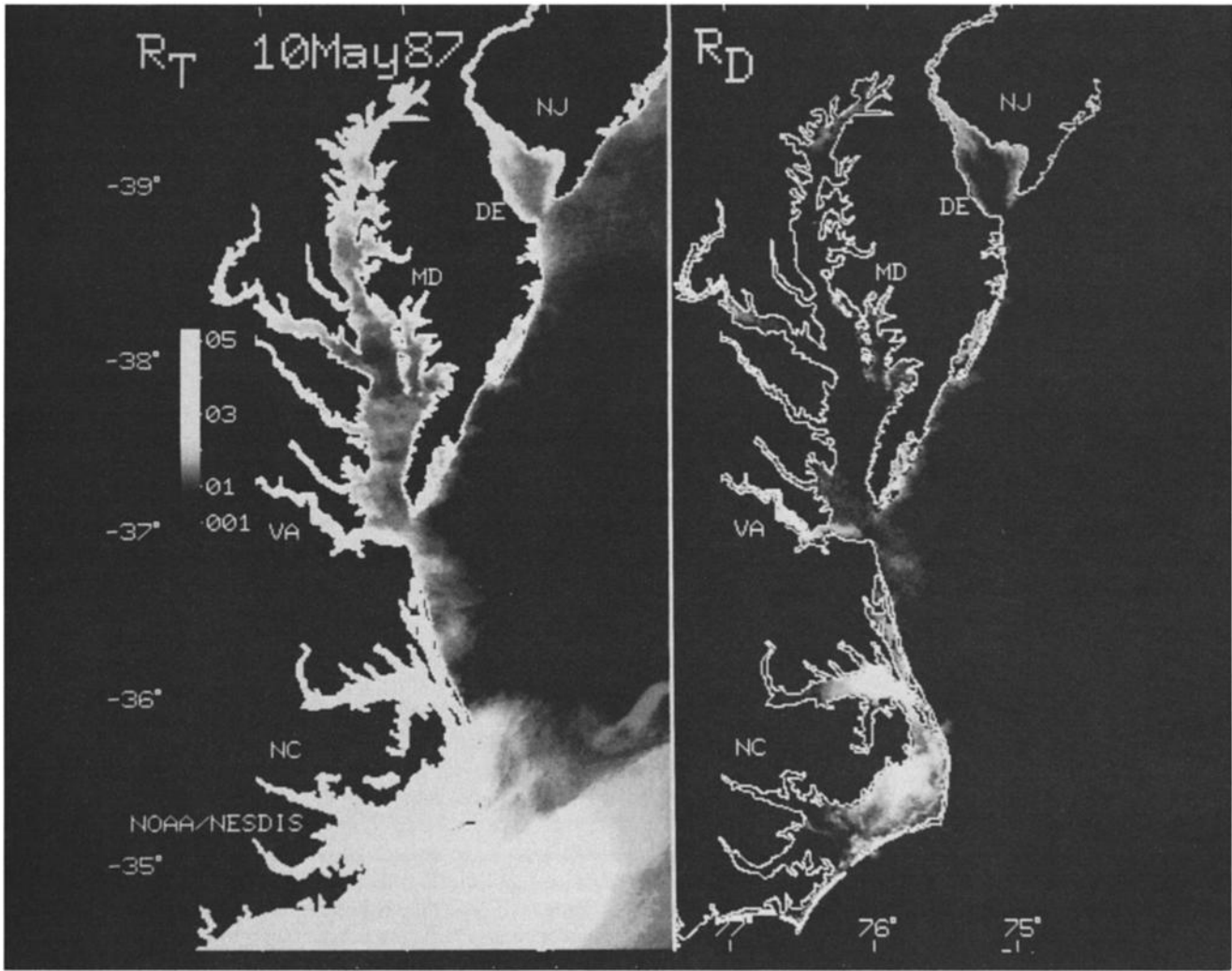
Fig. 4. Reflectance of the U.S. Middle Atlantic Bight on May 10, 1988 showing (left) $R_T$ and (right) $R_D$.
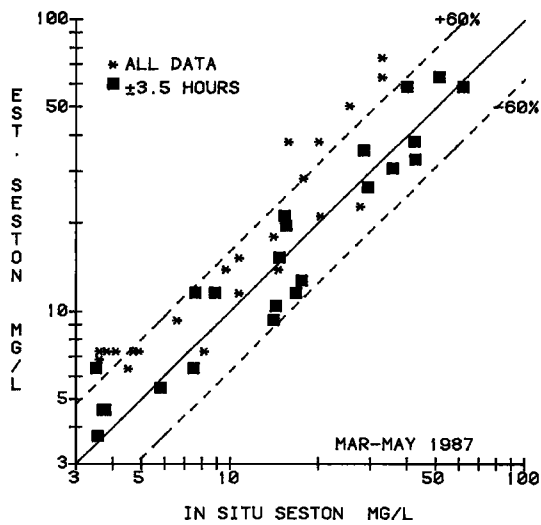


Fig. 5. Estimated $n_s$ (from $R_T$) versus in situ $n_s$. The solid line indicates identical values. Dashed lines show the 95% confidence interval ($\pm 60\%$) of estimated $n_s$ from the line of unity.
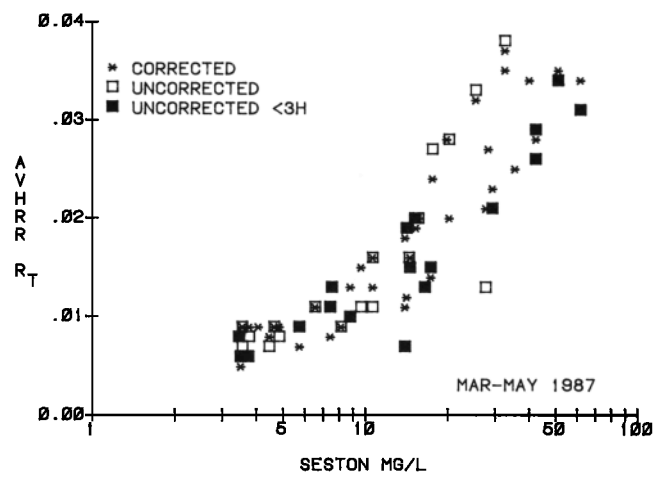
Fig. 6. Seston concentrations versus $R_T$ showing $R_T$ found using locations corrected for tidal transport and not corrected (i.e. the ship station location). Uncorrected <3H denotes values taken within 3.5 hours of an overpass.

TABLE 4. Sources of Variation Between Near-Simultaneous Samples

| | Reflectance | $n_s$, % |
|---|---|---|
| *Satellite Data* | | |
| Atmospheric error | <0.003 | <20 [a] |
| Digitization error | 0.007 | 5 |
| Positioning error and and pixel-scale variability | <0.002 | <15 [a] |
| *In Situ Data* | | |
| Sampling and analytical error in $n_s$ | | 10 |
| Subpixel variability at 500-m scale | | 7 |

[a] Calculated from $R_T$ for the linear portion of the curve in Figure 2.

sampling at 2-m depth. The bath was completely flushed every 2 min and drained from the bottom to remove depositing sediment. This exchange time acts as a moving average on the data, smoothing out variations of <2 min. The percent transmission was recorded every 30 s. At speeds of 10-15 knots (5.1-7.7 m/s), the ship covered 150-230 m between records, 600-920 m during the exchange time of the bath, and the width of a pixel (1.16 km) in 2.5 to 3.8 min. The transmission measurements were converted to beam attenuation coefficients (c), because c will vary in proportion to $n_s$ [*vande Hulst*, 1957], permitting its use as a surrogate for $n_s$.

The satellite pixel value would roughly correspond to the mean value of each 1.16-km segment of data along the track line (Figure 7). Within the pixel-sized segments, the maximum variation from the segment mean ranged from 1 to 23%. The mean of these variations for all blocks was 7%. The variations from the segment mean could represent the potential discrepancy caused by subpixel variability at a scale of about 300 m. Because of the smoothing effect of the bath, these results would not resolve most variability at scales of <300 m and thereby provide an extremely conservative estimate of the total subpixel variability. Higher-resolution data on beam transmission will provide more detail on the degree of the subpixel and pixel scale.

As much as 50% of the discrepancy between the data sets may result from sources other than the satellite data or algorithm. The atmospheric correction, digitization, and pixel positioning would produce variations of up to 25-40%. Subpixel variability and in situ processing could produce a minimum of another 17%. Errors in identifying the location of the sampled water (either from satellite or at the surface) would produce 0-20%. Therefore even when both data sets are completely error-free and calibrated for sediments of uniform composition, the problems of spatial variability and water movement will still produce potential discrepancies of 10-20% between the two data sets.
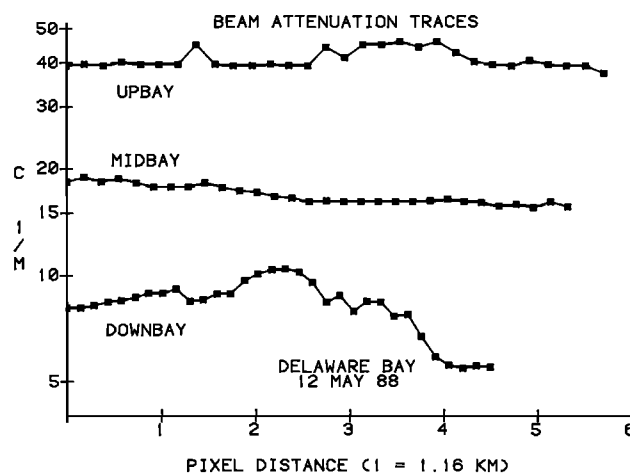


Fig. 7. Traces of beam transmission for Delaware Bay. The upbay trace started at 39°37', the midbay trace started at 39°16', and the downbay trace started at 38°59'. Distance is marked in pixel widths (1.16 km).

## Refinement and Applications to Other Estuaries

Using the coefficients presented in this paper, equation (2) can provide an initial estimate of the relative suspended sediment concentration in coastal waters having reflectances between 0.003 (1 mg/L) and 0.04-0.05 (60-100 mg/L). Because small variations in reflectance at higher values will be associated with large variations in $n_s$, these coefficients should not be extrapolated to higher concentrations. Evidence indicates, however, that (2) will apply to concentrations up to at least 200 mg/L when additional calibration data are used [*Stumpf*, 1988b]. Since the AVHRR sensors have shown some evidence of a decrease in sensitivity over time and since they require external calibration [*Abel et al.*, 1988], the coefficients to compute reflectance may have to be modified slightly for NOAA 9 data collected in other years (especially 1985 and early 1986).

Equation (2) represents a solution to the radiative transfer equation; this physical, rather than statistical, basis provides a physical reference to the coefficients. In statistically derived models, the coefficients have no physical meaning and so remain unique to the calibration dataset [e.g., *Khorram*, 1985]. However, the coefficients in (2) can be adjusted for different characteristics of the suspended materials in different areas. In areas where both reflectance and in situ suspended sediment measurements exist, the calculated parameters, $b_{bs}{}^*$ and $s^*$, can also provide an indication of similarities or differences in sediment type compared to that of Delaware Bay. An analysis of the parameters for the effects of variations in the relative optical grain size may ultimately be used to assess variations in grain size in estuaries.

The near-daily coverage of the AVHRR increases the probability that an overpass will coincide with some in situ sampling. Thus we may obtain improved calibrations of the remotely sensed data and a better concept of the differences or similarities between many different estuaries. Although the large pixel size limits investigations to estuaries wider than about 3 km, intercalibration with data collected from Landsat, SPOT, and other platforms could occasionally extend measurements into smaller estuaries or permit detection of events covering a small area.

The study of oceanic productivity and global sea surface temperatures has benefitted greatly from the application of physically based atmospheric corrections and models to satellite data. In estuaries, more emphasis should be placed on the same approach: the use of atmospherically corrected reflectances and standardized physical relationships to relate satellite observations to materials in the water. This approach could be used as a means of comparing estuaries and river plumes around the world.

## REFERENCES

Abel, P., G. R. Smith, R. H. Levin, and H. Jacobowitz, Results from aircraft measurements over White Sands, New Mexico, to calibrate the visible channels of spacecraft instruments, *Proc. Ocean Opt.*, *924*, 208-214, 1988.

Arthur, J. F. and M. D. Ball, Factors influencing the entrapment of suspended material in the San Francisco Bay - delta estuary, in *San Francisco Bay: The Urbanized Estuary*, edited by T. J. Conomos, pp.143-174, AAAS, Washington, D. C., 1979.

Bolt, Beranek, and Newmann, *RS/1 User's Manual, Version 10*, Cambridge, Mass., 1981.

Bukata, R. P., J. H. Jerome, J. E. Bruton, S. C. Jain, and H. H. Zwick, Optical water quality model of Lake Ontario, 1, Determination of the optical cross-sections of organic and inorganic particulates in Lake Ontario, *Appl. Opt.*, *20*, 1696-1703, 1981.

Cole, B. E., J. E. Cloern, and A. E. Alpine, Biomass and productivity of three phytoplankton size classes in San Francisco Bay, *Estuaries, 9(2)*, 117-125, 1986.

Curcio, J. A. and C. C. Petty, The near-infrared absorption spectrum of liquid water, *J. Opt. Soc. Am.*, *41(5)*, 302-314, 1951.

Curtin, T. B. and R. V. Legeckis, Physical observations in the plume region of the Amazon River during peak discharge, I, Surface variability, *Cont. Shelf Res.*, *6*, 31-51, 1986.

Durkee, P. A., The relationship between marine aerosol particles and satellite-detected radiance, Colo. State Univ., Ph.D. dissertation, *Atmos. Sci. Pap. 380*, 124 pp., Fort Collins, 1984.

Gagliardini, D. A., H. Karszenbaum, R. Legeckis, and V. Klemas, Application of Landsat MSS, NOAA/TIROS AVHRR, and Nimbus CZCS to study the La Plata River and its interaction with the ocean, *Remote Sens. Environ., 15*, 21-36, 1984.

Gordon, H. R., O. B. Brown, and M. M. Jacobs, Computed relationships between the inherent and apparent optical properties of a flat homogeneous ocean, *Appl. Opt., 14*, 417-427, 1975.

Gordon, H. R., D. K. Clark, J. W. Brown, O. B. Brown, R. H. Evans, and W. W. Broenkow, Phytoplankton pigment concentrations in the Middle Atlantic Bight: Comparison of ship determinations and CZCS estimates, *Appl. Opt., 22*, 20-33, 1983.

Griggs, M., Satellite measurements of tropospheric aerosols, *Adv. Space Res., 2*, 109-118, 1983.

Jain, S. C. and J. R. Miller, Algebraic expression for the diffuse irradiance reflectivity of water from the two-flow model, *App. Opt., 16*, 202-204, 1977.

Khorram, S., Development of water quality models applicable throughout the entire San Francisco Bay and delta, *Photogramm. Eng. Remote Sens., 51(1)*, 53-62, 1985.

Kidwell, K. B., NOAA polar orbiter data (TIROS-N, NOAA-6, NOAA-7, NOAA-8, NOAA-9, NOAA-10) users guide, Natl. Environ. Satell. Data and Inf. Serv., Natl. Oceanic and Atmos. Admin., Washington D.C., 1986. (Revised Jan. 1988.)

Klemas, V., M. Otley, W. Philpot, C. Wethe, R. Rogers, and N. Shah, Correlation of coastal water turbidity and circulation with ERTS-1 and Skylab imagery, in *Proceedings of the 9th International Symposim on Remote Sensing of Environment*, pp. 1297-1317, Environmental Research Institute of Michigan, Ann Arbor, 1974.

Lyzenga, D., C. Bostater, M. Stein, and A. Matteoda, High resolution spectral signatures of turbid coastal water: Implications for radiative transfer inversion models, (abstract), *Eos, Trans. AGU, 69(16)*, 379, 1988.

MacFarlane, N., and I. S. Robinson, Atmospheric correction of Landsat MSS data for a multidate suspended sediment algorithm, *Int. J. Rem. Sens., 5(3)*, 561-576, 1984.

Munday, J. C., and T. T. Alfoldi, Landsat test of diffuse reflectance models for aquatic suspended solids measurements, *Rem. Sens. Environ., 8*, 169-183, 1979.

Pennock, J. R., Chlorophyll distributions in the Delaware estuary: Regulation by light-limitation, *Est. Coast. Shelf Sci., 21*, 711-725, 1985.

Philpot, W. D., Radiative transfer in stratified waters: A single-scattering approximation for irradiance. *App. Opt., 26(19)*, 4123-4132, 1987.

Planet, W. G., Data extraction and calibration of TIROS-N/NOAA radiometers, *Tech. Memo. NESS 107 - Rev. 1*, Natl. Oceanic and Atmos. Admin., Washington, D.C., 1979 (revised 1988).

Ritchie, J. C., C. M. Cooper, and J. Yongqing, Using Landsat multispectral scanner data to estimate suspended sediments in Moon Lake, Mississippi, *Rem. Sens. Environ., 23*, 65-81, 1987.

Schubel, J. R., Distribution and transportation of suspended sediment in upper Chesapeake Bay, in *Environmental Framework of Coastal Plain Estuaries, Geol. Soc. America, Mem. Geol. Soc. Am. 133*, edited by B. W. Nelson, pp. 91-113, Geological Society of America, Boulder. Colo., 1972.

Sharp, J. H., C. H. Culberson, and T. M. Church, The chemistry of the Delaware estuary: General considerations, *Limnol. Oceanog., 27*, 1015-1028, 1982.

Strickland, J. D. H., and T. R. Parsons, A practical handbook of seawater analysis, *Bull. Fish. Res. Board Can., 167*, 310 pp., 1972.

Strong, A. E., and E. P. McClain, Improved ocean surface temperatures from space--comparisons with drifting buoys. *Bull. Am. Meteorol. Soc., 65*, 138-142, 1984.

Stumpf, R. P., Application of AVHRR satellite data to the study of sediment and chlorophyll in turbid coastal water, *Tech. Memo. NESDIS AISC 7*, 50 pp., Natl. Environ. Satell. Data, and Inf. Serv., Natl. Oceanic and Atmos. Admin,. Washington, D.C., 1987

Stumpf, R. P., Sediment transport in Chesapeake Bay during floods: Analysis using satellite and surface observations, *J. Coastal Res, 4(1)*, 1-15, 1988a.

Stumpf, R. P., Remote detection of suspended sediment concentrations in estuaries using atmospheric and compositional corrections to AVHRR data, in *Proceedings of the 21st International Symposium on Remote Sensing of Environment*, pp. 205-222, Environmental Research Institute of Michigan, Ann Arbor, 1988b.

Stumpf, R. P., and M. A. Tyler, Satellite detection of bloom and pigment distributions in estuaries, *Rem. Sens. Environ., 24(3)*, 385-404, 1988.

Tassan, S., and B. Sturm, An algorithm for the retrieval of sediment content in turbid coastal waters from CZCS data, *Int. J. Remote Sens., 7(5)*, 643-655, 1986.

U.S. Department of Commerce, Tidal current tables, Atlantic coast of North America, 243 pp., National Ocean Survey, Natl. Oceanic and Atmos. Admin., Rockville, Md., 1987.

vande Hulst, H. C., *Light Scattering by Small Particles*, John Wiley, New York, 1957.

Whitlock, C. H., L. R. Poole, J. W. Usry, W. M. Houghton, W. G. Witte, W. D. Morris, and E. A. Gurganus, Comparison of reflectance with backscatter and absorption parameters for turbid waters, *Appl. Opt., 20(3)*, 517-527, 1981.

J. R. Pennock, The University of Alabama, Marine Environmental Sciences Consortium, P. O. Box 369-370, Dauphin Island, AL 36528.

R. P. Stumpf, Office of Research Applications, NOAA NESDIS, Suitland Professional Center, Room 315, Washington, D. C. 20233.